

## Saturation-compensated measurements for fluorescence lifetime imaging microscopy

YIDE ZHANG, GENEVIEVE D. VIGIL, LINA CAO, AAMIR A. KHAN, DAVID BENIRSCHKE, TAHSIN AHMED, PATRICK FAY, AND SCOTT S. HOWARD\*

Department of Electrical Engineering, University of Notre Dame, Notre Dame, Indiana 46556, USA

\*Corresponding author: showard@nd.edu

Received 26 October 2016; revised 29 November 2016; accepted 29 November 2016; posted 30 November 2016 (Doc. ID 279389); published 23 December 2016

**Fluorophore saturation is the key factor limiting the speed and excitation range of fluorescence lifetime imaging microscopy (FLIM). For example, fluorophore saturation causes incorrect lifetime measurements when using conventional frequency-domain FLIM at high excitation powers. In this Letter, we present an analytical theoretical description of this error and present a method for compensating for this error in order to extract correct lifetime measurements in the limit of fluorophore saturation. We perform a series of simulations and experiments to validate our methods. The simulations and experiments show a  $13.2 \times$  and a  $2.6 \times$  increase in excitation range, respectively. The presented method is based on algorithms that can be easily applied to existing FLIM setups.** © 2016 Optical Society of America

**OCIS codes:** (170.3650) Lifetime-based sensing; (180.4315) Nonlinear microscopy; (190.4180) Multiphoton processes; (170.2520) Fluorescence microscopy.

<https://doi.org/10.1364/OL.42.000155>

Fluorescence lifetime imaging microscopy (FLIM) is a powerful tool for biomedical studies because it enables the measurement of important information such as the ion concentration, the dissolved oxygen concentration, the pH, and the refractive index, about the microenvironment surrounding living cells [1]. FLIM can be performed either in the time domain by time-correlated single photon counting [2–4] or in the frequency domain using lock-in detection [5–7]. In this Letter, we will only discuss the frequency-domain FLIM, which is attractive for its rapid acquisition, easy implementation, and reduced bandwidth requirements [5]. However, the speed and accuracy of FLIM is limited by fluorophore saturation, which causes nonlinearities such that the conventional FLIM methods using lock-in detection will no longer work [8]. To avoid the onset of saturation in FLIM, researchers limit the excitation intensity to a narrow range, which requires a longer integration time for a satisfactory signal-to-noise ratio, thus limiting the imaging speed [9]. Moreover, avoiding saturation in FLIM excludes the benefits introduced by fluorophore saturation, for it has

proven to be a valuable tool to implement super-resolution microscopy with spatial resolution beyond the diffraction limit [10–12].

In this Letter, we present an original frequency-domain FLIM method that exploits the nonlinear nature of fluorophore saturation to increase the excitation range. The two-level fluorophore model and mathematical descriptions of our method are presented. We perform a series of simulations and experiments to validate our model and method. A comparison in lifetime measurements is demonstrated between our FLIM method and the conventional one. The calibration and measurement errors of both methods are also discussed.

The fluorophore is modeled as a two-level system with absorption, stimulated emission, and radiative and nonradiative decays. The process is depicted in a Jablonski diagram in Fig. 1(a) with a ground singlet state,  $S_0$ , and excited singlet state,  $S_1$  [1]. We denote the probability of occupying the ground and excited singlet states as  $S_0(t)$  and  $S_1(t)$ , respectively, which are functions of time. To make this model applicable to both one-photon and multiphoton excitation, the absorption and stimulated emission rates are written as  $g_p \sigma_N \phi^N(t)$ , where  $\phi(t)$  is the incident photon flux,  $N$  denotes the number of excitation photons needed for a fluorophore to emit one photon ( $N = 1$  for one-photon excitation,  $N = 2$  for two-photon excitation, etc.),  $\sigma_N$  is the cross section for  $N$ -photon excitation, and  $g$  is the pulse gain factor which takes the temporal pulse profile of the excitation into account [13,14]. The radiative decay rate,  $1/\tau_r$ , and the nonradiative decay rate,  $1/\tau_{nr}$ , contribute to the fluorescence or phosphorescence with lifetime  $\tau$  concurrently. This model is an empirical abstraction of the dynamics of the singlet and triplet states and the intersystem crossing [15–17], and considers  $\tau_r$  and  $\tau_{nr}$  as effective parameters. A rate equation describing Fig. 1(a) can be written as

$$\frac{dS_1(t)}{dt} = g_p \sigma_N \phi^N(t) S_0(t) - g_p \sigma_N \phi^N(t) S_1(t) - \frac{S_1(t)}{\tau}. \quad (1)$$

The probabilities of occupying  $S_0$  and  $S_1$  must sum to unity,  $S_0(t) + S_1(t) = 1$ . The excitation irradiance,  $I(t)$ , is related to  $\phi(t)$  by  $I(t) = \phi(t)/\gamma$ , where  $\gamma = \lambda/(hc)$  depicts the reciprocal photon energy,  $h$  is Planck's constant,  $c$  is the velocity of

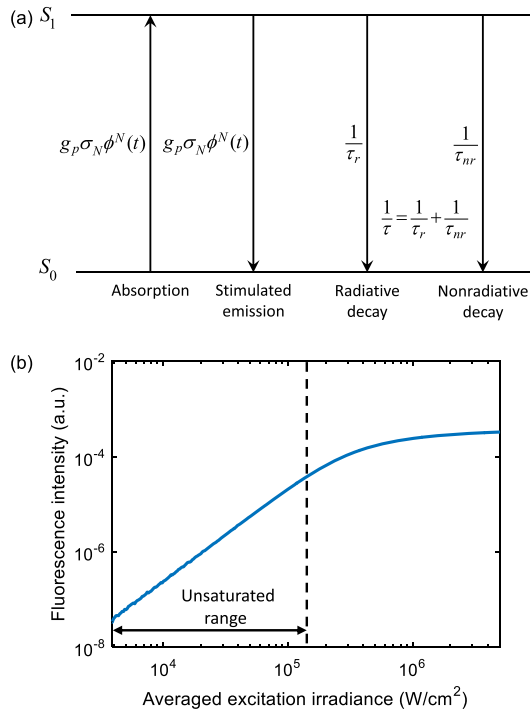


**Fig. 1.** (a) Jablonski diagram showing the two-level fluorophore model. (b) Numerical solution of Eq. (2) under two-photon excitation showing the saturation behavior.

light, and  $\lambda$  is the excitation wavelength. The fluorescence intensity,  $F(t)$ , is proportional to the probability of occupying the excited singlet state,  $S_1(t)$ . We denote  $F(t) = K S_1(t)$ , where  $K = \psi_F t_{ob} / \tau_r$ ,  $\psi_F$  is the fluorescence detection efficiency, and  $t_{ob}$  is the observation time. For a certain experimental condition,  $K$  is constant and needs to be calibrated for a precise lifetime measurement under saturation. From Eq. (1), we have

$$\frac{dF(t)}{dt} = K g_p \sigma_N \gamma^N I^N(t) - 2 g_p \sigma_N \gamma^N I^N(t) F(t) - \frac{F(t)}{\tau}. \quad (2)$$

Although factors such as higher excited singlet and triplet states and photobleaching are not included in this model, it can precisely describe the fluorophore saturation behavior, which can be seen by the simulated excitation-fluorescence relation in Fig. 1(b). Figure 1(b) is obtained by numerically solving the differential equation (2) under two-photon excitation, where conventional FLIM is usually limited to the unsaturated range denoted in the figure, as the excitation outside of this range leads to nonlinear behaviors and incorrect lifetime measurements.

To measure the lifetime evenly in the case of fluorophore saturation, an original frequency domain FLIM method is presented. In this method, the excitation irradiance  $I(t)$  is intensity-modulated at an angular frequency of  $\omega$ . Thus, the  $N$ -photon fluorescence  $F(t)$  is periodic with period  $T = 2\pi/\omega$ . Based on the periodicity of  $I(t)$ ,  $I^N(t)$ , and  $F(t)$ , we can describe them with the Fourier series  $I^N(t) = \sum_{m=-\infty}^{+\infty} p_m \exp(im\omega t)$ ,  $F(t) = \sum_{n=-\infty}^{+\infty} q_n \exp(in\omega t)$ , where  $p_m$  and  $q_n$  are the Fourier coefficients. From Eq. (2), for the Fourier coefficients with index  $k$ , we know that

$$q_k \left( ik\omega + \frac{1}{\tau} \right) = K g_p \sigma_N \gamma^N p_k - 2 g_p \sigma_N \gamma^N \sum_{l=-\infty}^{+\infty} p_l q_{k-l}. \quad (3)$$

Based on the property of the Fourier series, the convolution term  $\sum_{l=-\infty}^{+\infty} p_l q_{k-l}$  in Eq. (3) is the Fourier coefficient of the product of the temporal signals  $I^N(t)$  and  $F(t)$ . We define

$$r_k = \sum_{l=-\infty}^{+\infty} p_l q_{k-l} = \frac{1}{T} \int_0^T I^N(t) F(t) \exp(-ik\omega t) dt. \quad (4)$$

Therefore, Eq. (3) can be written as

$$q_k \left( ik\omega + \frac{1}{\tau} \right) = g_p \sigma_N \gamma^N (K p_k - 2 r_k). \quad (5)$$

Define

$$s_k = K p_k - 2 r_k \quad (6)$$

and then we have

$$\begin{aligned} |q_k| \exp(i\Delta q_k) \sqrt{(k\omega)^2 + \frac{1}{\tau^2}} \exp[i \tan^{-1}(k\omega\tau)] \\ = g_p \sigma_N \gamma^N |s_k| \exp(i\Delta s_k). \end{aligned} \quad (7)$$

Based on the phase equality of Eq. (7), we get

$$\Delta q_k + \tan^{-1}(k\omega\tau) = \Delta s_k \quad (8)$$

and the fluorescence lifetime can be obtained as

$$\tau = \frac{1}{k\omega} \tan(\Delta s_k - \Delta q_k). \quad (9)$$

Note that this method can be easily reduced to the conventional frequency domain FLIM phase method by eliminating the  $r_k$  term in Eq. (6); thus, we get  $s_k = K p_k$ , and the lifetime is calculated from the phase difference between the excitation and fluorescence, i.e.,

$$\tau = \frac{1}{k\omega} \tan(\Delta p_k - \Delta q_k). \quad (10)$$

We perform a series of simulations and experiments to validate the presented saturation-compensated FLIM method [Eq. (9)] and compare it with the conventional one [Eq. (10)]. We only show the two-photon excitation case ( $N = 2$ ) and extract the lifetime from the first harmonics of the involved signals ( $k = 1$ ). An extension to other cases ( $N \neq 2$ ,  $k \neq 1$ ) is straightforward. The simulation is based on numerically solving the rate equation [Eq. (2)] of the two-level model in Matlab and applying Eqs. (3)–(10) to calculate lifetimes. The simulation parameters are set as follows:  $\tau = 1.6$  ns,  $\tau_r = \tau/0.3$ ,  $\psi_F = 0.02$ ,  $t_{ob} = 200$  ns,  $g_p = 38690$ ,  $\sigma_2 = 2 \times 10^{-48}$  cm<sup>4</sup>s,  $\lambda = 800$  nm,  $f_{mod} = 62.5$  kHz, and  $\omega = 2\pi f_{mod}$ . Poisson noise was added to the simulated signals before lifetime calculations. The experiment is performed on a custom-built multiphoton FLIM similar to the one we used in [18]. A mode-locked Ti:sapphire laser (Spectra Physics Mai Tai BB, 800 nm, 100 fs, 80 MHz) was used as the laser source and its intensity was modulated by an electro-optic modulator (Thorlabs EO-AM-NR-C1), whose waveform was controlled by a function generator. The excitation irradiance was varied by a continuously variable neutral density filter controlled by a stepper motor. The excitation illumination was filtered through a longpass filter to block ambient light from entering the microscope. The excitation beam was expanded

by a telescope to overfill the back aperture of an objective lens (Nikon CFI APO NIR, 40 $\times$ , 0.8 NA), which created a diffraction-limited spot inside the cuvette. We used a deionized water-dissolved [Ru(dpp)<sub>3</sub>]<sup>2+</sup> nanomicelle probe as our sample in the cuvette [19]. The fluorescence  $F(t)$  was epi-collected by the objective lens, reflected by a dichroic mirror, filtered through a set of bandpass and shortpass filters to eliminate residual excitation, and detected by a photomultiplier tube (PMT) [Hamamatsu H7422PA-40]. The excitation  $I(t)$  was monitored by a photodetector (Thorlabs PM100D). Both excitation and emission signals were digitized by a data acquisition card (National Instruments PCI-6110). Lifetime calculations using Eqs. (9) and (10) were performed in real time in LabView (National Instruments).

Before measuring lifetime, two calibration steps are needed. First, the system phase offset is calibrated by measuring the phase difference between  $I^N(t)$  and  $F(t)$  in a near-zero lifetime sample (Rhodamine B, 1000 $\times$  shorter in lifetime than [Ru(dpp)<sub>3</sub>]<sup>2+</sup>) or, alternatively, a reflective surface, and is converted to a relative temporal shift which will be applied to actual temporal data in experiments. Second, the coefficient  $K$  should be determined. It is calibrated by performing two measurements with unmodulated excitation ( $\omega = 0$ ). Based on Eq. (5), when  $\omega = 0$ , under the two-photon excitation ( $N = 2$ ) and DC lock-in ( $k = 0$ ), we have

$$q_0 = \tau g_p \sigma_2 \gamma^2 (K p_0 - 2r_0). \quad (11)$$

The two measurements provide two sets of detectable quantities  $p_0^a, q_0^a, r_0^a$  and  $p_0^b, q_0^b, r_0^b$ . With Eq. (11),  $K$  can be determined by

$$K = 2 \frac{r_0^b q_0^a - r_0^a q_0^b}{p_0^b q_0^a - p_0^a q_0^b}. \quad (12)$$

The numerically simulated result is presented in Fig. 2. As the averaged excitation irradiance increases, the calculated lifetimes from the saturation-compensated [Eq. (9)] and conventional [Eq. (10)] methods show distinct features; the lifetimes calculated conventionally start to deviate from their true value 1.6  $\mu$ s by 10% when the excitation irradiance is larger than  $1.37 \times 10^5$  W/cm<sup>2</sup>, while the lifetimes obtained

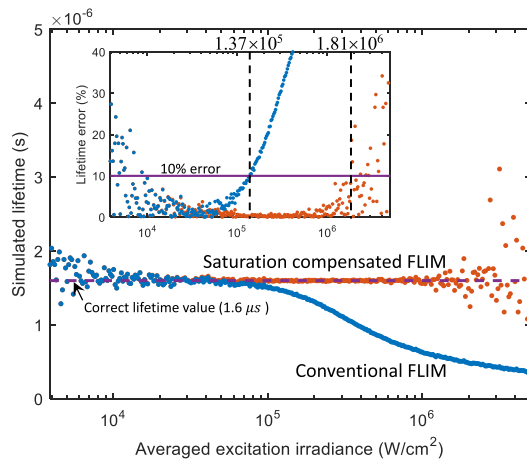


**Fig. 2.** Lifetime results simulated from saturation-compensated [Eq. (9)] and conventional [Eq. (10)] FLIM methods, based on the numerical simulation of the two-level model under two-photon excitation. Inset: lifetime errors relative to the correct lifetime value (1.6  $\mu$ s).

from the saturation-compensated FLIM method stay on the correct value within 10% error until the excitation exceeds  $1.81 \times 10^6$  W/cm<sup>2</sup>. This distinction shows a  $13.2 \times$  increase in the excitation range using the saturation-compensated FLIM method. A notable feature of the proposed saturation-compensated method is that the error increases significantly at the intensity beyond the 10% error excitation range. An explanation is that the phase in the tangent function in Eq. (9) approaches  $\pi/2$  as the intensity increases; therefore, the noise is amplified by the divergence of the tangent function.

In the experiment, the [Ru(dpp)<sub>3</sub>]<sup>2+</sup> nanomicelle sample was held at a lifetime of  $\tau = 1.6 \mu$ s by air saturating the solution and sealing the cuvette. The modulation frequency was  $0.1/\tau = 62.5$  kHz since a  $0.1/\tau$  modulation produced the best lifetime measurement signal-to-noise ratio [18,20]. We set the integration time to 500 ms to reduce the error introduced by the noise. Figure 3 shows the measured lifetimes using the saturation-compensated [Eq. (9)] and conventional [Eq. (10)] FLIM methods. Note that the unit of experimentally measured power in Fig. 3 is mW, which is different from the units W/cm<sup>2</sup> in Figs. 1 and 2 which are based on single fluorophore simulations. The result shows that an excitation intensity larger than 8.06 mW can cause a measurement error larger than 10% if the conventional method is used. However, under saturation conditions, the saturation-compensated FLIM method presented in this Letter provides correct lifetime measurements within 10% error up to an excitation intensity of 21.0 mW, demonstrating a  $2.6 \times$  increase in the excitation range compared to the conventional method.

Although the simulation and experiment both show the improvement in the excitation range using the saturation-compensated FLIM method, there is a disparity between the  $13.2 \times$  and  $2.6 \times$  improvements provided by the simulation and experiment, respectively. The disparity can also be seen from the slopes of the conventional FLIM lifetimes under saturation conditions. A possible explanation is that the simulation is based on a single fluorophore, while the experimentally detected fluorescence comes from a mixture of saturated and unsaturated fluorophores within the focal volume [21]. Alternatively, the two-level model does not reflect photobleaching,

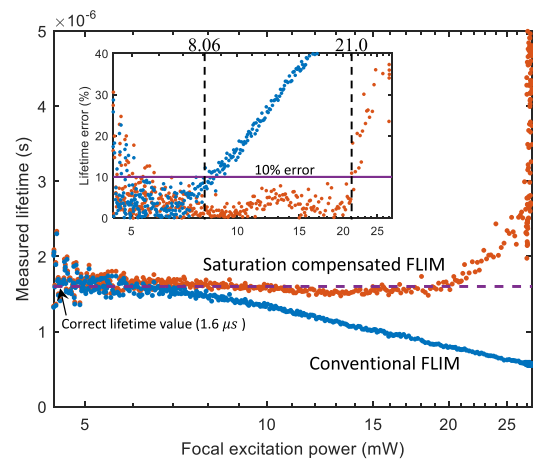


**Fig. 3.** Lifetime results measured with saturation-compensated [Eq. (9)] and conventional [Eq. (10)] FLIM methods, based on the two-photon excitation experiment. Inset: lifetime errors relative to the correct lifetime value (1.6  $\mu$ s).

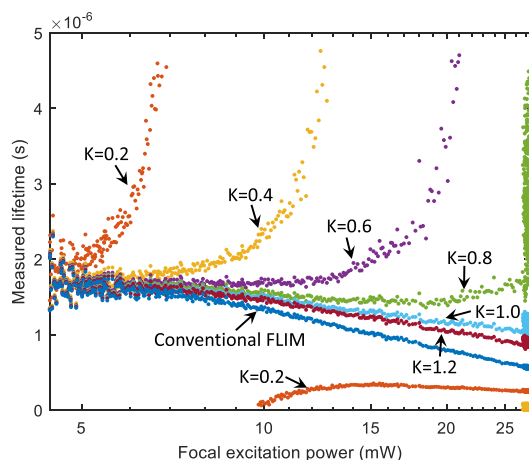


**Fig. 4.** When the coefficient  $K$  is varied, the experimentally measured lifetimes using the saturation-compensated FLIM method show distinct features.

which can be easily observed in actual experiments [22]. On the other hand, the precise calibration of the coefficient  $K$  in the experiment can be difficult due to the noise. Figure 4 shows how different values of  $K$  cause distinct lifetime features. If a calibration is not performed correctly, the incorrect  $K$  coefficient can result in inferior performance. When the calibration described in Eq. (12) cannot provide a satisfactory result, an offline  $K$  calibration, i.e., adjusting  $K$  until obtaining a good lifetime performance, should be considered.

The measurement errors of the saturation-compensated and conventional FLIM methods are analyzed by experimentally measuring the lifetimes at 19 different excitation powers. At each excitation level, the lifetime measurements were repeated for 1000 times, with the integration time of 10 ms. The obtained lifetime means and standard deviations are presented as error bars in Fig. 5. Note that the excitation range in Fig. 5 is narrower than the one in Fig. 3 because the shorter integration time introduces more error in the calibration of  $K$ . The relative

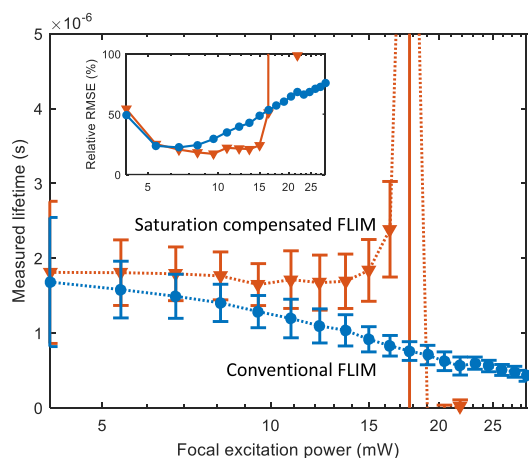


**Fig. 5.** Error analysis of the saturation-compensated and conventional FLIM methods. The error bars indicate a standard deviation from the mean of the measured lifetimes. Inset: the ratio of the RMSE and the actual value of the lifetime.

root-mean-square errors (RMSEs) as a function of the excitation power for each method are shown in the inset. The saturation-compensated FLIM method demonstrates another advantage over the conventional one by maintaining a relatively small RMSE over the extended excitation range.

In conclusion, we have demonstrated an original frequency-domain FLIM method that exploited the nonlinear nature of fluorophore saturation to increase the excitation range. Instead of avoiding the saturation limit, our method shows good performance beyond the saturation limit and offers the possibility of exploiting the benefits such as super-resolution imaging provided by fluorophore saturation. The model and method have been validated by simulations and experiments. Since the only difference between our saturation-compensated method and the conventional method lies in the way the signals are processed while no hardware modification is needed, it is easy and straightforward for researchers interested in FLIM to incorporate this method in their experiments.

**Funding.** National Science Foundation (NSF) (CBET-1554516).

## REFERENCES

- H. C. Gerritsen, A. Draaijer, D. J. van den Heuvel, and A. V. Agronskaia, *Handbook Of Biological Confocal Microscopy*, J. Pawley, ed. 3rd ed. (Springer, 2006), pp. 516–534.
- D. O'Connor, *Time-Correlated Single Photon Counting* (Academic, 2012).
- J. Qi, Y. Shao, L. Liu, K. Wang, T. Chen, J. Qu, and H. Niu, *Opt. Lett.* **38**, 1697 (2013).
- X. Y. Dow, S. Z. Sullivan, R. D. Muir, and G. J. Simpson, *Opt. Lett.* **40**, 3296 (2015).
- J. Philip and K. Carlsson, *J. Opt. Soc. Am. A* **20**, 368 (2003).
- M. Zhao and L. Peng, *Opt. Lett.* **35**, 2910 (2010).
- S. S. Howard, A. Straub, N. G. Horton, D. Kobat, and C. Xu, *Nat. Photonics* **7**, 33 (2012).
- S. P. Poland, N. Krstajić, J. Monypenny, S. Coelho, D. Tyndall, R. J. Walker, V. Devauges, J. Richardson, N. Dutton, P. Barber, D. D.-U. Li, K. Suhling, T. Ng, R. K. Henderson, and S. M. Ameer-Beg, *Biomed. Opt. Express* **6**, 277 (2015).
- A. M. D. Lee, H. Wang, Y. Yu, S. Tang, J. Zhao, H. Lui, D. I. McLean, and H. Zeng, *Opt. Lett.* **36**, 2865 (2011).
- M. G. L. Gustafsson, *Proc. Natl. Acad. Sci. USA* **102**, 13081 (2005).
- K. Fujita, M. Kobayashi, S. Kawano, M. Yamanaka, and S. Kawata, *Phys. Rev. Lett.* **99**, 228105 (2007).
- A. D. Nguyen, F. Dupont, A. Bouwens, F. Vanholsbeeck, D. Egrise, G. Van Simaey, P. Emplit, S. Goldman, and S.-P. Gorza, *Opt. Express* **23**, 22667 (2015).
- C. Eggeling, A. Volkmer, and C. A. M. Seidel, *ChemPhysChem* **6**, 791 (2005).
- C. Xu and W. W. Webb, *J. Opt. Soc. Am. B* **13**, 481 (1996).
- E. Gatzogiannis, X. Zhu, Y.-T. Kao, and W. Min, *J. Phys. Chem. Lett.* **2**, 461 (2011).
- X. Zhu and W. Min, *Chem. Phys. Lett.* **516**, 40 (2011).
- Y. Yonemaru, M. Yamanaka, N. I. Smith, S. Kawata, and K. Fujita, *ChemPhysChem* **15**, 743 (2014).
- Y. Zhang, A. A. Khan, G. D. Vigil, and S. S. Howard, *Opt. Express* **24**, 20862 (2016).
- A. A. Khan, S. K. Fullerton-Shirey, and S. S. Howard, *RSC Adv.* **5**, 291 (2015).
- Y. Zhang, A. A. Khan, G. D. Vigil, and S. S. Howard, *J. Opt. Soc. Am. A* **33**, B1 (2016).
- W. R. Zipfel, R. M. Williams, and W. W. Webb, *Nat. Biotechnol.* **21**, 1369 (2003).
- G. H. Patterson and D. W. Piston, *Biophys. J.* **78**, 2159 (2000).